Dynamic effects on transition between two-dimensional regular and Mach reflection of shock waves in an ideal steady supersonic free stream

K. NAIDOO†, B. W. SKEWS

School of Mechanical, Aeronautical and Industrial Engineering, University of the Witwatersrand, Johannesburg, 2050, South Africa

(Received Submitted 22 October 2010; revised 8 January 2011; accepted 29 January 2011)

There have been numerous studies on the steady state transition criteria between regular and Mach reflection of shock waves generated by a stationary, two-dimensional wedge in a steady supersonic flow, since the original shock wave reflection research by Ernst Mach in 1878. The steady, two-dimensional transition criteria between regular and Mach reflection are well established. There has been little done to consider the dynamic effect of a rapidly rotating wedge on the transition between regular and Mach reflection. This paper presents the results of an investigation on the effect of rapid wedge rotation on regular to Mach reflection transition in the weak and strong-reflection ranges, with the aid of experiment and computational fluid dynamics. The experimental setup includes a novel facility to rotate a pair of large aspect ratio wedges in a 450 mm $\times$ 450 mm supersonic wind tunnel at wedge rotation speeds up to 11000 deg/s. High-speed images and measurements are presented. Numerical solution of the inviscid governing flow equations was used to mimic the experimental motion and to extend the investigation beyond the limits of the current facility to explore the influence of variables in the parameter space. There is good agreement between experiment and numerical simulation. This paper includes the first experimental evidence of regular to Mach reflection transition beyond the steady state detachment condition in the weak and strong-reflection ranges. It also presents results of simulations for dynamic regular to Mach reflection transition which show a difference between the sonic, length scale and detachment conditions. This paper includes experimental evidence of Mach to regular reflection transition below the steady state von Neumann condition.

Key Words: dynamic shock wave reflection, dynamic transition, dynamic Mach stem, rapid wedge rotation

1. Introduction

Consider the shock wave system generated by a flight vehicle in steady, level supersonic flight as illustrated in figure 1. The regular and Mach reflection possible on the ground plane as well as the transition conditions between idealised versions of these two configurations (figure 2) has been researched since the early work of Ernst Mach in 1878. The primary interest in the last 30 years has been the establishment of the steady state

† Council for Scientific and Industrial Research, Defence Peace Safety and Security, Aeronautics Systems Competency, Pretoria, South Africa, 0001

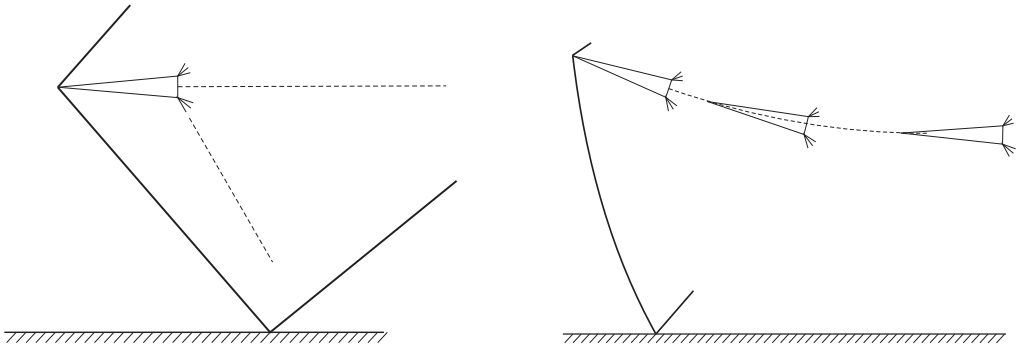

FIGURE 1. Simplified schematic of (a) steady shock wave reflection with the flight vehicle in steady, level flight and (b) dynamic shock wave reflection when the vehicle increases its pitch orientation rapidly

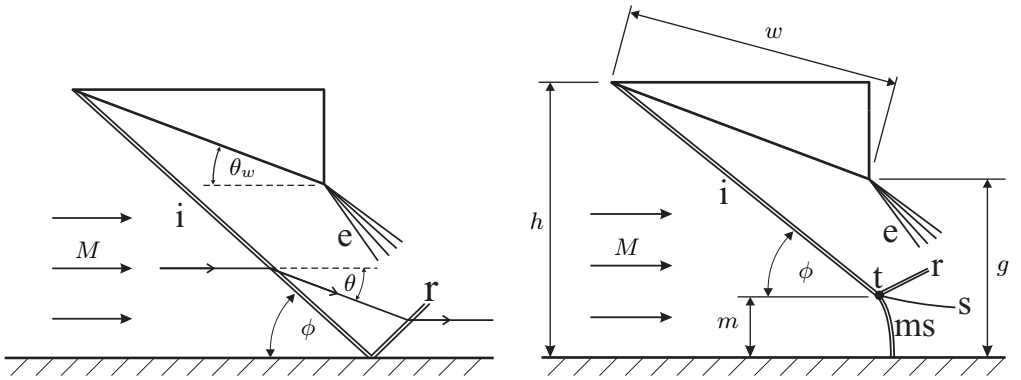

(a) Regular reflection (b) Mach reflection

FIGURE 2. Simplified schematics of regular and Mach reflection generated by a wedge in a steady supersonic free stream

transition criteria between regular and Mach reflection in the strong-reflection range, i.e. $Mach \geqslant 2.202$ for air with a ratio of specific heats, $\gamma = 1.4$. To date there has been little published research that is relevant to the dynamic development of the reflection pattern as the flight vehicle increases its pitch orientation rapidly.

Typically, steady shock wave reflection research has considered the shock wave pattern in the reference frame of a simplified wedge for the purpose of fundamental analysis and experiment. Since the gas medium ahead of the reflection pattern has no velocity relative to the ground plane in reality, there is no boundary layer ahead of the reflection point. Therefore, in the reference frame of the wedge, the ground plane is approximated by an idealised, frictionless surface. For the range of positive incidence of the wedge for which the incident shock wave is attached to the wedge leading edge, there are two possible reflection patterns, viz. a two-shock system or regular reflection (figure 2(a)) and a three-shock system or Mach reflection (figure 2(b)). In the case of a regular reflection (RR) the incident wave, "i", deflects the free stream flow towards the reflection plane and the reflected wave, "r", returns the flow parallel to the reflection plane. In the case of Mach reflection (MR) the incident wave, reflected wave, Mach stem, "ms", and the shear layer, "s" meet away from the reflection plane at the triple point, "t". Figure 2 also includes

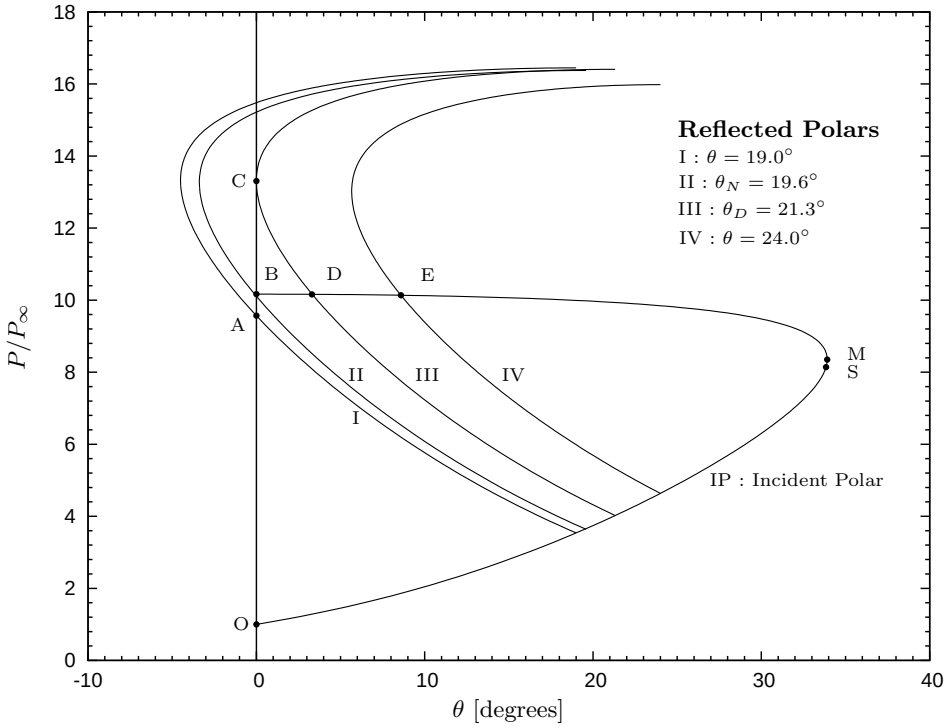

FIGURE 3. Critical pressure-deflection shock polars for steady reflection at $M = 2.98$

definitions for the flow deflection angle, θ, wedge incidence, θ_w, shock incidence, ϕ, Mach stem height, m, wedge chord, w, as well as the leading and trailing edge separation from the reflection plane, g and h.

Steady state transition criteria between RR and MR generated by a wedge of infinite span in a steady supersonic flow are derived by taking into account local flow conditions at the reflection/triple point only and were published by Ben-Dor (2007). As the wedge incidence is increased gradually from an initial, steady RR, such that the reflection pattern approximates steady state at each point in time, there is a critical incidence beyond which transition to MR occurs. As the wedge incidence is decreased gradually from an initial, steady MR, such that the reflection is approximately steady at each instant, there is a critical incidence below which transition to RR occurs.

Pressure-deflection shock polars are a convenient, effective, graphical means of representing the analytical solution for ideal, steady, two-dimensional RR and MR. They are presented, only briefly here, to illustrate the derivation of the steady RR ↔ MR transition criteria. Ben-Dor (2007) may be consulted for a detailed exposition and supporting theory. Critical polars for the steady case with free stream Mach number, $M = 2.98$ are shown in figure 3. Polar "IP" represents the static pressure rise, P/P_∞, that can be achieved through an incident oblique shock wave at $M = 2.98$ for a range of flow deflections, θ. P_∞ is the free stream static pressure and P is the static pressure downstream of the incident wave. In the ideal case, the incident wave deflects the flow parallel to the wedge surface and θ equals θ_w. The flow deflection at point "M" is the maximum deflection possible by an oblique wave. For larger values of θ, the incident oblique wave is detached. The largest pressure rise possible through an oblique wave is at zero flow de-

flection, corresponding to the normal shock solution, i.e. the intersection of "IP" with the vertical axis at point "B". The sonic point on "IP", labelled "S", separates the incident polar into supersonic and subsonic segments where the downstream flow is supersonic or subsonic respectively ("O" to "S" : supersonic segment; "B" to "S" : subsonic segment). For smaller values of flow deflection, there are two solutions for each value of θ and the downstream flow can be either subsonic or supersonic. Usually, in practice, the downstream flow is supersonic as in the case of interest here and the segment of "IP" between "S" and "O" is applicable.

Now consider the reflection of the incident oblique wave on an ideal, horizontal reflection plane in a steady supersonic free stream. The reflection is either RR or MR. The flow condition downstream of the reflection/triple point is determined by superimposing the polar for the reflected wave on "IP". The flow deflection by the incident wave locates the origin of the reflected polar on the incident polar. Four sample reflected polars, labelled "I", "II", "III" and "IV" are constructed on "IP" and they correspond to analytical solutions for the pressure rise through the reflection and/or triple point at $\theta = 19.0°, 19.6°, 21.3°$ and $24.0°$ respectively. For RR, as depicted in figure 2(a), the incident wave turns the free stream away from the wedge surface and the reflected wave returns the flow parallel to the reflection plane, i.e. a zero net flow deflection. Therefore, the flow state downstream of the reflection point is given by the intersection of the reflected polar with the vertical axis on the graph which corresponds to a zero net flow deflection. RR is theoretically possible as long as the reflected polar intersects the vertical axis. The maximum flow deflection point on reflected polar "III", point "C", is tangent to the vertical axis and is termed the detachment condition corresponding to θ_D or ϕ_D. For $\theta > \theta_D$ the reflected wave of a RR cannot turn the flow parallel to the reflection plane at the reflection point and only MR is possible e.g. polar "IV" at $\theta = 24.0°$ and point "E" gives the flow state downstream of the triple point. Steady MR in a steady supersonic flow is possible as long as the reflected polar intersects the incident polar to the right hand side of the vertical axis. Polar "II" corresponds to the smallest flow deflection for which MR is theoretically possible at $M = 2.98$. At this condition, the pressure rise through the reflection/triple point is the same as the normal shock solution for "IP" at point "B" and is termed the von Neumann condition or the mechanical equilibrium condition corresponding to θ_N or ϕ_N. If RR $\leftrightarrow$ MR transition were to occur at this point, there is a continuous and smooth change in pressure rise through the reflection/triple point through transition. At $\theta = 19.0°$, the flow state downstream of the reflection point is "A" and only RR is possible. The range of flow states between the von Neumann and detachment conditions is termed the dual solution domain and is a function of Mach number for a particular gas. At the sonic condition (not shown here), corresponding to θ_S or ϕ_S, the sonic point on the reflected polar is on the vertical axis and the flow downstream of the reflection point is $M = 1.0$. This is very close to the detachment condition and the difference is usually neglected in practice, e.g. at $M = 2.98$, $\theta_S = 21.2°$ and $\theta_D = 21.3°$.

In air, with $\gamma = 1.4$, there is no von Neumann condition below $M = 2.202$. The reflected polar corresponding to the detachment condition at $M = 1.93$ is shown in figure 4 as an example. Hornung (1986) defines "weak" and "strong" reflections in terms of the location of the maximum deflection point on the reflected polar at the detachment condition with respect to the normal shock solution on the incident polar. For example, in figure 4, point "A", lies below the normal shock solution of the incident wave and the reflection is termed a weak reflection. In contrast, at $M = 2.98$, point "C" in figure 3 lies above the normal shock solution of the incident wave and the reflection is termed a strong reflection. At $M = 2.202$ the point of maximum flow deflection on the reflected wave at

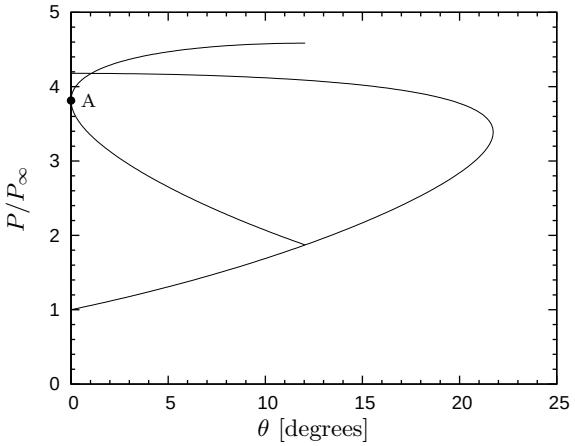

FIGURE 4. Pressure-deflection shock polar for a reflection at the detachment condition at $M = 1.93$

the detachment condition is co-incident with the normal shock solution. Accordingly, $M < 2.202$ is referred to as the weak-reflection range and $M > 2.202$ is referred to as the strong-reflection range.

Perhaps, the significance of whether the reflection is regular or Mach in the dual solution domain is best considered at this point. Consider the polars in figure 3. The difference in pressure across the reflection point between the von Neumann condition at point "B" and the detachment condition at point "C" is approximately $3.1 \times P_\infty$. This difference increases to $12.9 \times P_\infty$ at $M = 4.0$. The point of transition is important in determining the maximum pressure rise through the reflection and may be applied to investigations of aircraft sonic boom, supersonic intake design, etc. Azevedo & Liu (1993) highlighted the relatively large contribution of the subsonic region behind the Mach stem of a MR to acoustic levels in comparison to the otherwise supersonic flow as applicable to supersonic engine intakes and supersonic vehicle design. Perhaps, this condition could be avoided or at least taken into account with a knowledge of the point of transition.

Ben-Dor (2007) may be consulted for a detailed review of the steady, two-dimensional RR ↔ MR transition criteria. In the ideal case, for air at $M \geqslant 2.202$, transition depends on the direction of wedge incidence change. RR and MR are possible in the dual solution domain between the von Neumann and detachment conditions. ϕ_N is the smallest shock incidence at which MR is theoretically possible and ϕ_D is the largest shock incidence at which RR is possible. The length scale criterion or information condition proposed by Hornung et al. (1979) stated that RR → MR transition occurs at the point when flow conditions change such that there is communication of the wedge length scale to the reflection point (through the expansion fan). In the ideal, steady case, this is when the flow immediately downstream of the reflection point first goes sonic, i.e. $M = 1.0$ at ϕ_S. Since the flow downstream of the reflection point is supersonic for $\phi < \phi_S$ there can be no communication of the wedge length scale to the reflection point below ϕ_S. This also happens to be very close to ϕ_D, beyond which RR is not possible. It so happens in the ideal, steady case that the earliest incidence at which the length scale is visible to the reflection point is negligibly close to the incidence at which a RR is no longer possible. In this case there has been no need to differentiate between the two as they are so close. If the wedge incidence is decreased from an initial, steady MR, the Mach

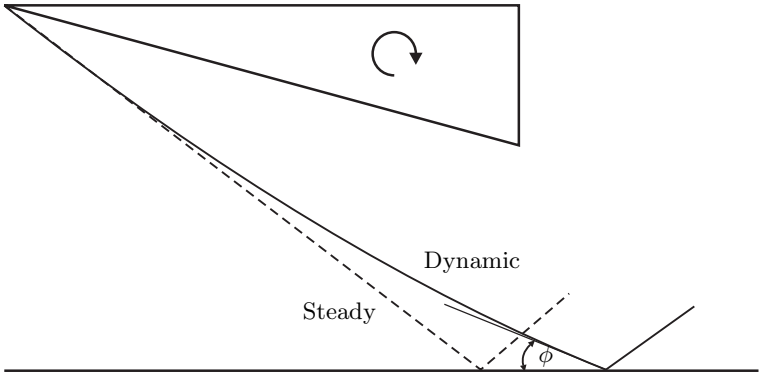

FIGURE 5. Typical curvature observed in flow computations by Khotyanovsky et al. (1999) and Felthun & Skews (2004) for rapid increasing wedge incidence

stem height decreases, and MR is maintained until the von Neumann condition in the strong-reflection range and until the detachment condition in the weak-reflection range.

In summary, in the strong-reflection region, steady RR → MR transition occurs at the sonic/detachment condition and the reverse transition occurs at the von Neumann condition (Ben-Dor (2007)). This wedge-angle induced hysteresis phenomenon was confirmed experimentally by Ivanov et al. (2003) and various researchers with numerical simulation (see Ben-Dor (1999)). In the weak-reflection range, the point of transition is the detachment condition in both directions.

The theoretical, transition criteria were derived specifically for steady flows and are invalid for the dynamic case of interest. Felthun & Skews (2004) simulated a rapidly rotating, two-dimensional wedge in a $M = 3.0$ free stream and predicted significant deviation from the steady state transition criteria. They also observed curvature on the incident wave as illustrated in figure 5.

This paper presents results from a novel experiment designed to observe the dynamic effect of rapid wedge rotation on RR → MR transition in the weak and strong-reflection ranges. Euler computations were used to model the experiment and were also applied beyond the capability of the current facility to explore the sensitivity of the dynamic effect to other variables, i.e. pivot point, initial incidence and rotation speed. Computations were also used to investigate the dynamic RR → MR transition mechanism. Experimental measurements and computations for the dynamic MR → RR transition in the strong-reflection range are also presented.

For the sake of clarity, when the incident shock is curved in the dynamic case, ϕ will refer to the shock incidence angle at the reflection point as indicated in figure 5. The wedge and shock incidence at transition is labelled θ_{WT} and ϕ_T respectively. A dimensionless parameter, M_E, is defined to quantify the wedge rotation speed in terms of the free stream acoustic velocity, viz. $M_E = V_E/a_\infty$, where V_E is the wedge edge speed of the leading or trailing edge depending on the rotation centre and a_∞ is the free stream acoustic speed. With respect to the experiment, the reflection pattern in the streamwise vertical plane of symmetry is of primary interest. All measurements are made on this vertical symmetry plane and all results will refer to the measurements made in this plane unless otherwise stated.

2. Background

2.1. *Early origins of rapid wedge rotation*

There are a handful of publications that investigate dynamic effects on shock wave reflections in steady flows. Most focus on the prediction and observation of the hysteresis phenomenon for the steady case in the strong-reflection range.

Hornung, Oertel & Sandeman (1979) first proposed the length scale transition criterion for RR → MR transition in steady flows, viz. the sonic condition in ideal flows. This hypothesis was supported by results from pseudosteady experiments in a shock tube in which RR → MR transition was observed close to the sonic condition. In their shock tube experiments, an incident planar shock travels through a stationary gas at constant speed over a plane wedge. The flow is termed pseudosteady because the RR that develops as the leading shock passes over the wedge is self-similar in time and the flow in the immediate vicinity of the reflection point in the reference frame of the reflection point is steady.

Henderson & Lozzi (1979) also presented data that showed the persistence of RR beyond the von Neumann condition with the diffraction of strong shocks over surfaces in an unsteady flow field. In their shock tube experiments the wedge is concave and the shock incidence decreases as the shock passes over the wedge. In the reference frame of the reflection point the flow is changing with time and is considered unsteady.

These observations in pseudosteady and unsteady flows and the compelling physical arguments of Hornung et al. (1979) led them to propose an incidence-induced hysteresis experiment in the dual solution domain for the steady case. It was predicted that RR → MR transition would occur at the sonic or detachment condition and the reverse transition would occur at the von Neumann condition.

Hornung & Robinson (1982) conducted a set of experiments in which the wedge incidence of a symmetric double wedge configuration, was increased and decreased gradually through the dual solution domain in steady, free stream conditions at $M = 2.84$, 3.49, 3.98 and 4.96. No hysteresis was observed and RR ↔ MR transition was observed repeatedly at the von Neumann condition, irrespective of the direction of incidence change. It was suggested that disturbances in the flow were sufficient to cause early RR → MR transition at the von Neumann condition.

Since 1995, there have been a number of publications on computational prediction and the experimental observation of hysteresis in the dual solution domain. Ben-Dor (2007) includes a detailed review and bibliography of milestone publications in this field. Various computations with numerical solution of the Euler and Boltzmann equations supported the feasability of hysteresis (Vuillon, Zeitoun & Ben-Dor (1999), Chpoun & Ben-Dor (1995), Ivanov, Gimelshein & Beylich (1995), Ivanov et al. (1996), Ben-Dor (1999)), due to the absence of free stream perturbations in the simulations. Flow simulations were successful in predicting hysteresis, but there was a failure to observe this phenomenon in an experiment.

Computations were done to determine the effect of free stream density, pressure and velocity perturbations by Ivanov et al. (1998), Khotyanovsky, Kudryavtsev & Ivanov (1999), and Kudryavtsev et al. (2002). Results supported the hypothesis that free stream perturbations present in the experiment, not in the flow computations, would cause early transition to MR.

Hornung (1997) suggested that it was possible that RR → MR transition would not be influenced by free stream disturbances in the experiment if the wedges were rotated sufficiently rapidly into the dual solution domain. He proposed establishing a steady RR before rotating the wedge rapidly into the dual solution domain, terminating the wedge motion just below the wedge incidence corresponding to detachment, θ_D. This could

prevent information of the wedge length scale from reaching the reflection point until the wedge was well into the dual solution domain. This is the earliest known published requirement for a rapid wedge rotation experiment, though its roots lie in the analysis of the steady problem.

The first experiment to consider this idea was published by Mouton & Hornung (2008), in which a single wedge of an asymmetric wedge arrangement was rotated very rapidly into the dual solution domain at $M = 4.0$. Though the wedge arrangement was asymmetric the transition criteria were recalculated as per the method published by Li, Chpoun & Ben-Dor (1999). The measurements supported the hypothesis made by Hornung (1997). Rapid wedge rotation did indeed delay transition to MR. RR persisted further into the dual solution domain for increasing wedge rotation speeds, but not up to the detachment condition.

2.2. *Computational simulation of wedge vibration and impulsive wedge rotation*

Prior to the experiments by Sudani et al. (2002), Ivanov et al. (2003) and Mouton & Hornung (2008), hysteresis was an elusive phenomenon for experimentalists. Markelov, Pivkin & Ivanov (1999) and Khotyanovsky et al. (1999) performed various numerical studies to determine the potential contribution of impulsive wedge rotation and high frequency vibration to this phenomenon.

Markelov et al. (1999) investigated the effect of wedge vibration on RR $\rightarrow$ MR transition with impulsive and periodic wedge oscillations. A steady, initial RR was established at $M = 4.96$ just below the detachment condition before the wedge was rotated impulsively at a constant rotation speed for 1° about its trailing edge. Dynamic flow features were observed, but none significant enough to trigger transition. However, impulsive rotation about the wedge leading edge did generate dynamic effects to the extent that it did cause transition. Periodic oscillations were also simulated to determine the minimum wedge oscillation frequencies required to trigger transition for various initial angles (oscillation amplitude = 1°). The simulated frequencies were in the order of magnitude of vibration frequencies of their facilities and these results supported the possibility that wedge vibration could contribute to the difference between experiment and simulation in terms of transition in the dual solution domain.

Concurrently, Khotyanovsky et al. (1999) investigated the effect of continuous rapid wedge rotation on the point of transition with Euler CFD on moving meshes. In contrast to the work by Markelov et al. (1999), Khotyanovsky et al. (1999) considered larger movements of the wedge. Rather than to investigate the dynamic phenomena generated by a rapidly rotating wedge, the objective of the study was to determine the maximum permissible wedge rotation speed that could be used in simulation without introducing dynamic effects. Wedges were rotated about the trailing edge at $M_T = 0.0002, 0.002, 0.01, 0.1$ in a $M = 5.0$ free stream, where $M_T = w\omega/U_\infty$ (w = wedge chord; ω = wedge rotation speed [rad/s]; U_∞=free stream speed). At $M_T = 0.1$ there was significant curvature on the incident wave as illustrated in figure 5, but in all instances ϕ_T was close to ϕ_D. No dynamic effect on the point of transition was reported.

While the work of Markelov et al. (1999) and Khotyanovsky et al. (1999) investigated rapid wedge rotation with particular focus on the implications for the steady case, Felthun & Skews (2004) specifically investigated the dynamics of the rapidly rotating wedge case. The wedge was rotated impulsively about its leading edge at various rotation speeds for increasing and decreasing incidence at $M = 3.0$ using Euler computations. Resultant trailing edge speeds were between 1 and 10 percent of the free stream acoustic speed. RR $\rightarrow$ MR transition was delayed beyond detachment. Curvature was generated on the incident wave and transition was delayed further for increasing rotation speeds for the

range of rotation speeds investigated. They also observed a lag between the steady and unsteady wave system as illustrated in figure 5. Felthun & Skews (2004) also investigated dynamic MR → RR transition at $M = 3.0$ briefly. Rapid wedge rotation resulted in MR → RR transition below the von Neumann condition.

The experiment documented in this paper was set up, in part, to verify the dynamic effect on transition reported by Felthun & Skews (2004). In addition, the investigation is extended to study the effect of rapid rotation on transition in the weak-reflection range.

3. Experimental method

All experiments were conducted in the blow-down supersonic wind tunnel at the Council for Scientific and Industrial Research (CSIR) in South Africa. The tunnel has a 450 mm × 450 mm test section and has a free stream speed range between $M = 0.6$ and 4.3. Maximum available blow times range from 15 to 30 seconds depending on the experiment flow conditions. Apart from a single honeycomb mesh in the settling chamber there are no additional mechanisms to reduce the turbulence levels of the flow in the test section. Mach number control is achieved with a flexible nozzle that is actuated with a series of hydraulic actuators. As transition in the strong-reflection range is dependent on the level of free stream turbulence in the facility (Ben-Dor et al. (2002)), it was necessary to determine the steady transition criteria for $M \geqslant 2.202$ in the CSIR facility.

In an experiment, the ideal slip wall or reflection plane is usually generated with a symmetric double wedge configuration. The symmetric arrangement of the wedges about a horizontal image plane sets up a perfectly rigid, frictionless, adiabatic wall. This ensures that the reflection point is not contaminated by a boundary layer that would develop on a surface in the tunnel. The constructed rig (figure 6) consists of two large aspect ratio wedges arranged and actuated symmetrically about a horizontal reflection plane. The use of finite aspect ratio wedges, as opposed to wedges spanning the entire test section, are necessary to avoid the complex shock-boundary layer interaction on the test section window, which will produce confusing features on the schlieren images. The approach adopted in this investigation was to actuate both wedges symmetrically rather than a single wedge with corrected, theoretical transition criteria to account for the asymmetry.

Skews (1997, 2000) highlighted the issue of three-dimensional influences, from the wedge tip corner signal, on the reflection pattern in the vertical plane of symmetry. It was shown that transition between RR and MR in the vertical plane of symmetry approaches the steady, theoretical criteria, provided the wedge aspect ratio, b/w (where b is the wedge span), is above a critical value. Each wedge (chord, w=40.0 mm) has $b/w = 4.25$ and this is sufficient to ensure two-dimensional RR ↔ MR transition for $2.0 < M < 4.0$.

While the steady state point of transition approximates the two-dimensional transition condition for a large aspect ratio wedge, Ivanov et al. (2001) demonstrated with experiment and numerical solution that the Mach stem height generated in the vertical centre plane of a finite aspect ratio wedge is always less than the two-dimensional Mach stem height for the same incident shock wave incidence. Figure 7 shows the close agreement between the three-dimensional Euler CFD predictions of Ivanov et al. (2001) and their measurements from experiments with the finite aspect ratio wedge. This agreement established confidence in their two-dimensional Mach stem predictions with Euler CFD. The difference in Mach stem height between the two and three-dimensional result for the same shock incidence must be considered when comparing computed results with measurements from experiment.

The wedge pivot point was maintained as close to the trailing edge as possible and was

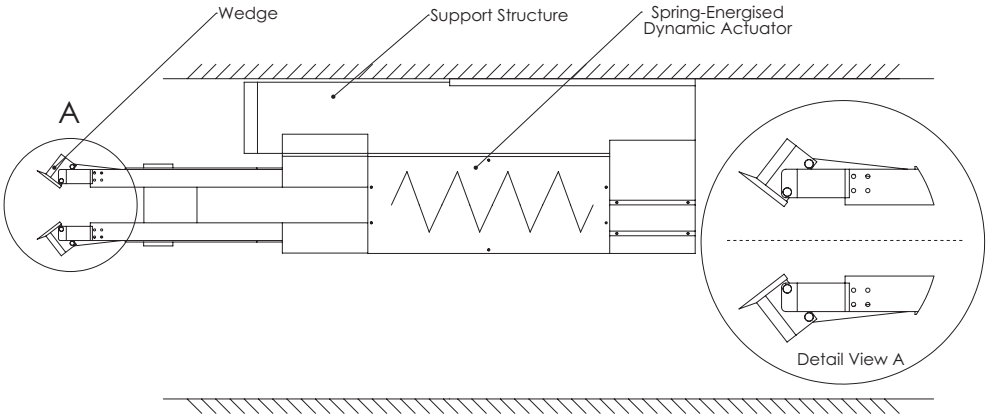

(a)

(b)

FIGURE 6. (a) Schematic and (b) photograph of the rig used for the dynamic experiments

selected to minimise the vertical movement of the trailing edge. The vertical movement of the trailing edge between wedge incidence, $\theta_w = 2.0°$ and $\theta_w = 25°$ is approximately 2.1% of the wedge chord. This variation is small, but its effect on transition is addressed later in this article with numerical simulation. The trailing edge separation, g, from the symmetry plane, was calculated to prevent the intersection of the expansion fan with the reflection point ($g/w \approx 0.6$ for all experiments).

The wedges were rotated gradually, with a servo motor, between 5.0 and 10 deg/s to generate steady state data. This rotation speed is sufficiently small such that the reflection pattern is approximately steady at each point in time. The wedges were rotated at larger rotation speeds with a spring-driven actuator to investigate the dynamic case. The actuator is assembled to achieve either rapid increasing or decreasing incidence.

Wedge rotation speeds that were used in simulations by Felthun & Skews (2004) resulted in wedge trailing edge speeds up to 10% of the free stream acoustic speed. The wedge was started impulsively (with an initial, established steady RR) and rotated at a constant rotation speed. In a typical supersonic blow down wind tunnel at $M = 3.0$, using air stored at 300.0 K, with $w = 40.0$ mm, this required starting the wedge impul-

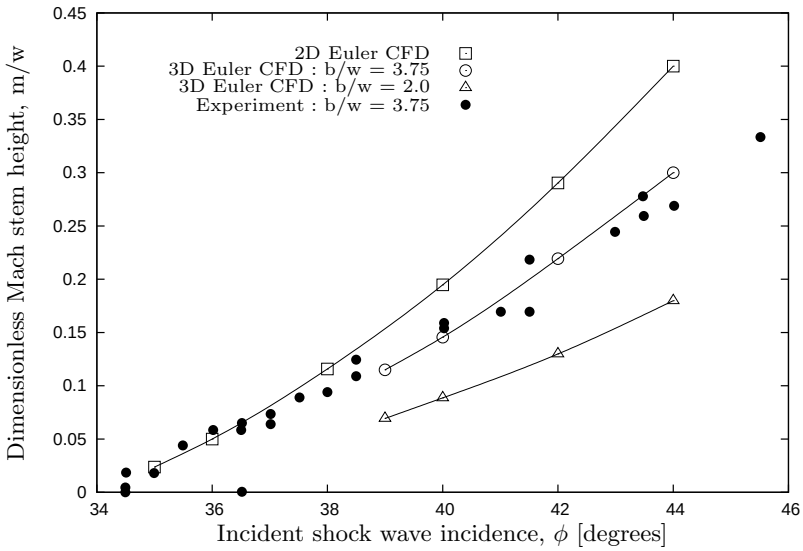

FIGURE 7. Two and three-dimensional Mach stem measurements from experiments and Euler predictions published by Ivanov et al. (2001) for a static wedge at $M = 4.0$, $g/w = 0.56$

sively and rotating it at a constant rate of approximately 30000 deg/s. Evidently, the validation of this type of numerical simulation with an experiment is not possible as it requires infinite acceleration at startup. Only finite acceleration could be considered in the experiment and this has been mimicked in the computations.

Various concepts were considered to realise the rotation speeds required, viz. spring-driven, electric, dynamic impact, pyrotechnics, pneumatics and hydraulics. As these experiments were the first of their kind in the CSIR tunnel, a spring-driven mechanism was considered primarily for the sake of simplicity and cost. A pair of compression springs were designed to generate an average $M_E = 0.01$ over a 25° rotation range. With an initial spring load of 1000N, the drive train is accelerated at approximately 1000m.s^{-2} and the motion is completed in approximately 6.0 ms. Depending on the experiment flow conditions a maximum instantaneous $M_E \approx 0.033$ was achieved, i.e. approximately 11000 deg/s. During the experiments, the tunnel and rig were operated remotely by a test team. At tunnel startup the wedges and spring system were locked with a custom designed latch system. After the flow stabilized at tunnel startup, the latch was released and the drive train was accelerated to achieve the required wedge rotation. A previous, unsuccessful, version of the rig was designed to achieve approximately 30000 deg/s in the required range. This was considerably larger and prevented tunnel startup due to the excessive blockage. Due to the significantly larger actuator forces it also raised concerns of safety during operation and was abandoned.

Flow visualization was achieved with a standard z-type schlieren system (Settles (2001)) and imaging was done with the Photron Ultima APX-RS high-speed camera. The camera has a 10-bit CMOS sensor with 1024 × 1024 pixels, with a pixel size of 17μm. In the steady state, baseline experiments, images were recorded at 250 fps (1024 × 1024 pixel resolution) and images from the dynamic experiments were captured at 10000 fps (512 × 512 pixel resolution). A calibration grid was used to correct image co-ordinates for any distortion in the image. The orientation of a line on the schlieren image may be measured within approximately ±0.3°. Uncertainty in non-dimensional Mach stem height measure-

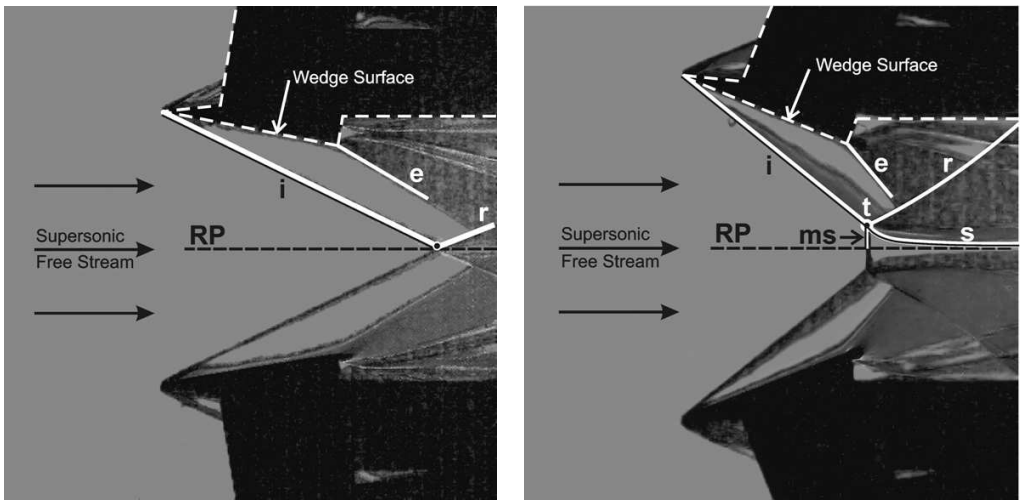

(a) (b)

FIGURE 8. Identification of pertinent flow features on schlieren images for (a) RR and (b) MR

ment is estimated at $\delta m/w = \pm 0.004$. Uncertainty in tunnel Mach number is estimated at approximately $\delta M = \pm 0.03$.

Two sample images from an experiment are presented in figure 8 to highlight the pertinent flow features on the wedge vertical plane of symmetry for RR and MR. Only the critical features above the reflection plane, "RP", are annotated. The annotations are consistent with those in figure 2. The incident wave, "i", the reflected wave, "r", Mach stem, "ms" and the shear layer, "s" meet at the triple point, "t" and the leading edge of the expansion is labelled "e". A white dashed line is used to highlight the wedge and rig outline.

4. Computational method

Numerical solution of the two-dimensional Euler equations were used to model the dynamic experiments and to extend the investigation beyond the capability of the existing facility to investigate the effect of pivot point, initial incidence and rotation speed on dynamic transition. An Euler CFD code was developed by Felthun (see Felthun & Skews (2004)) specifically for the solution of moving boundary problems in compressible flows and was previously used to simulate the rapidly rotating wedge.

The code is a vertex centred, arbitrary Lagrangian Eulerian finite volume scheme for unstructured triangular meshes. The Euler equations are solved with second-order accuracy. AUSM+ as formulated by Liou (1996) is implemented for the calculation of convective fluxes across cell interfaces. Node redistribution during boundary movement is implemented every time step with Laplacian smoothing. A mesh adaption routine was implemented to avoid excessive element deformation. The mesh adaption routine includes point insertion (for mesh refinement), edge collapsing (for mesh coarsening) and edge swapping (to optimise element quality). The in-house code was not optimised for solver speed, and Fluent V 12.0 was used for all steady state, inviscid flow calculations. Fluent V 12.0 has a compressible, density-based solver for the Euler and Navier-Stokes equations with adaptive refinement for the resolution of flow field gradients. First-order accuracy on triangular meshes was used.

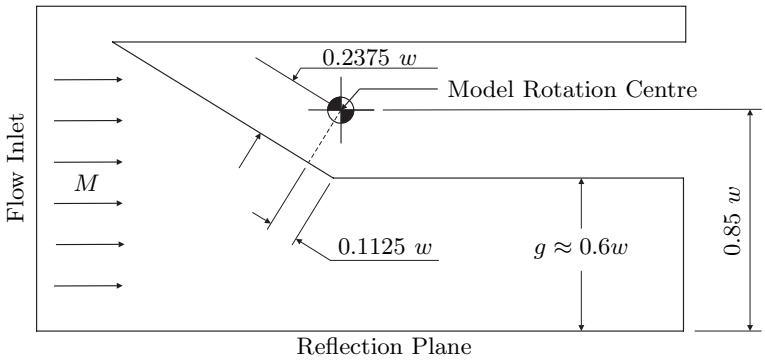

FIGURE 9. Schematic of computational model for simulation of the experiment

Figure 9 illustrates the flow domain boundaries of the grid for the experimental model. As the flow at the trailing edge is supersonic, the geometry downstream of the wedge was not modelled. As the wedge wake flow was not modelled, the exit dimensions change during the simulation. The flow was modelled as inviscid and all solid surfaces were modelled as "slip" walls.

4.1. *Grid sensitivity*

Fluent V 12.0 was used for all steady state simulations and the in-house Euler code was used for all dynamic simulations. A grid sensitivity study was performed on a static, two-dimensional wedge with $g/w = 0.56$ and $\phi = 40.0°$ at $M = 4.0$ in Fluent to determine the sensitivity of computed Mach stem height to grid element size. Ivanov et al. (2001) published the result of a two-dimensional Euler calculation of the Mach stem height for this configuration (see figure 7). Figure 10(a) shows the convergence of computed Mach stem height with the reduction in minimum element size, d. There is also close agreement to the predicted Mach stem height published by Ivanov et al. (2001).

In addition, simulations of a rapidly rotating wedge, with varying minimum element size were done with the in-house Euler code to determine the dependence of the computed dynamic RR → MR transition point on minimum mesh element size. A steady RR was established at an initial wedge incidence, $\theta_{wi} = 19.0°$, in a $M = 2.98$ free stream and the wedge incidence was increased rapidly at $M_E = 0.1$ until transition to MR. The rotation point was the same as the model in the experiment as shown in figure 9. The variation of ϕ_T with minimum element size is shown in figure 10(b). The difference in ϕ_T with the two finest grid resolutions is approximately 0.1°. At zero element size, the extrapolated $\phi_T \approx 40.57°$, 0.03° less than ϕ_T with the finest grid. Uncertainty in shock incidence measurement from flow field contours is estimated at approximately $\delta\phi = \pm 0.2°$.

4.2. *Incidence-induced hysteresis test*

In the incidence-induced hysteresis test, originally proposed by Hornung et al. (1979), a steady RR is established below ϕ_N and the wedge incidence is increased gradually until transition to MR. The wedge incidence is subsequently decreased until transition to RR. Ideally, RR → MR transition must occur at ϕ_D as there are no free stream disturbances in the flow simulation and the reverse transition must occur at ϕ_N. Felthun & Skews (2004) previously demonstrated the ability of the in-house Euler code to model this test case at $M = 3.0$. This was repeated here at $M = 2.98$ and results are presented in table 1.

A steady RR is established at $\phi < \phi_N$ and the wedge incidence is increased at

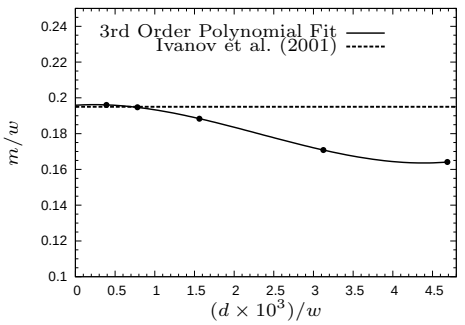

(a) Computed Mach stem height variation with minimum element size in Fluent at $\phi = 40.0°$, $M = 4.0$, $g/w = 0.56$. The solid line is a third-order polynomial fit to the data and is used to extrapolate m/w at zero d.

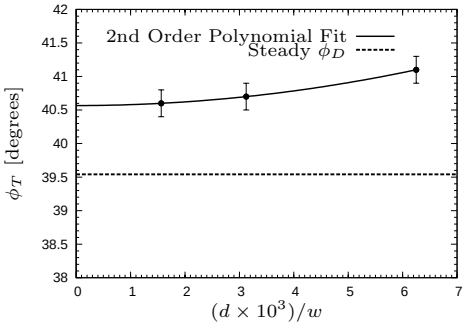

(b) Variation of computed ϕ_T with minimum element size with the in-house Euler code for $M_E = 0.1$ at $M = 2.98$. The solid line is a second-order polynomial fit to the data and is used to extrapolate ϕ_T at zero d.

FIGURE 10. Results from CFD grid sensitivity assessment for a static and dynamic simulation

	Computed ϕ_T	Theoretical ϕ_T
RR → MR transition	39.7°	$\phi_D = 39.5°$
MR → RR transition	37.3°	$\phi_N = 37.5°$

TABLE 1. Computed values for ϕ_T for the incidence-induced hysteresis test at $M = 2.98$ in comparison to steady state, theoretical values for RR ↔ MR transition

$M_E = 0.001$ such that there is no observable dynamic effect on the reflection pattern. RR was maintained through the dual solution domain and transition to MR occurred approximately 0.2° beyond ϕ_D. The wedge incidence is subsequently reduced at $M_E = 0.001$ and transition to RR was observed approximately 0.2° below ϕ_N. The deviation from ϕ_D and ϕ_N is within the value of uncertainty for shock incidence measurement documented in section 4.1.

5. Experimental results for dynamic regular to Mach reflection transition

Experiments to observe the dynamic RR → MR transition of interest were conducted in the weak and strong-reflection ranges at $M = 1.93$ and 2.98 respectively. The spring-driven actuator was installed to increase wedge incidence rapidly on latch release. Table 2 includes measured test conditions, viz. M, stagnation temperature (T_O), stagnation pressure (P_O) and the initial shock incidence (ϕ_i). Selected high-speed images from both experiments are presented in figures 11 and 13. Zero time corresponds to the image frame just before any wedge movement is visible on the high-speed images. The measured wedge motion and the streamwise movement of the reflection/triple point, x/w, is included in figures 12 and 14. The motion after the reflected wave of the MR intersects the wedge surface is not of interest here and was not analysed. Each frame before this time includes a value of time, t, as well as θ_w and ϕ. Figure 8 may be consulted to identify important features on the reflection pattern, viz. incident wave, reflected wave, reflection point, triple point, shear layer and the leading edge of the expansion fan. Images from both

M	P_O [kPa]	T_O [K]	ϕ_i [degrees]
1.93	232.0	302.7	35.5
2.98	474.0	302.3	23.2

TABLE 2. Experiment test conditions for dynamic RR → MR transition experiments, $g/w \approx 0.6$

experiments at $M = 1.93$ and 2.98 contain a similar sequence of events and the following qualitative description is applicable to both experiments, unless otherwise specified.

After tunnel startup a steady, initial RR is established (see figures 11(a) and 13(a)) after which time the latch mechanism restraining the actuation load is released. The rotation of the wedges about their pivot points is indicated. Initially, as the wedges rotate, there is little movement of the reflection point as the measurements show in figures 12(b) and 14(b). Both graphs show a distinct upstream movement only after approximately 2.5 - 2.6 ms of wedge motion. As the wedge incidence increases, transition to MR occurs and the triple point moves upstream. The Mach stem and the shear layer of the MR is visible in figures 11(c) and 13(c). In particular, at $M = 2.98$, the streamwise speed of the triple point after transition is different from the streamwise speed of the reflection point before transition and is evident from the change in gradient after transition in figure 14(b). As the wedge incidence increases further, the reflected wave of the MR intersects the wedge surface (figure 11(e) and 13(e)) and the wave system disgorges. The wedge motion terminates and a steady disgorged wave is established as seen in figures 11(f) and 13(f). The motion of interest is completed in approximately 4.5 ms at $M = 1.93$ and in approximately 5.5 ms at $M = 2.98$.

The speed of the reflection point at transition is used to calculate the effective local free stream speed at the reflection point at transition and the steady, analytical transition criteria are corrected accordingly. The shock incidence at the corrected von Neumann and detachment conditions will be referred to as ϕ_{NC} and ϕ_{DC} respectively in the rest of the manuscript. The measured test conditions in table 2 and wedge motion were used as inputs to the Euler simulations.

5.1. *Weak-reflection range*

The measurements from experiments and results from computations are presented in table 3 and figure 15(a). The solid lines in figure 15(a) are second-order polynomial fits through each data set and are used to extrapolate ϕ_T at zero m/w. The experimental and computed ϕ_T for the steady case are within 0.2° of ϕ_D. In the dynamic experiment, the wedge achieved an instantaneous rotation speed ($\approx$ 6300.0 deg/s) that resulted in $M_E = 0.02$ at the point of transition. The average M_E up to the point of transition was approximately 0.011. The rapid rotation delayed transition in the experiment and simulation of the experiment beyond ϕ_{DC} by approximately $1.2° - 1.3°$. Values of ϕ_T from the dynamic experiment and simulation of the experiment are within 0.1° of each other. As expected (and discussed by Ivanov et al. (2001)), there is the difference in Mach stem growth between the two-dimensional computed result and the three-dimensional experimental measurement for the steady case. This characteristic is also evident in the dynamic case. The close agreement between experiment and computation lends confidence to the ability of the computational method to predict dynamic transition.

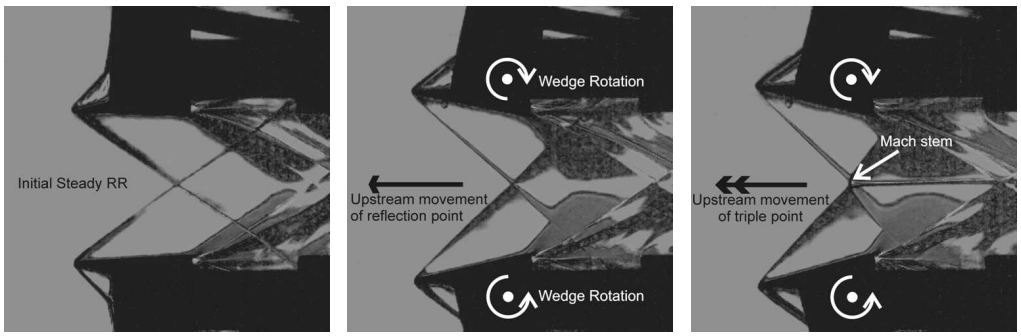

(a) t=0.0 ms, $\theta_w = 2.4°$, $\phi = 35.5°$ (b) t=3.4 ms, $\theta_w = 12.4°$,$\phi = 42.6°$ (c) t=3.8ms, $\theta_w = 15.0°$, $\phi = 45.8°$

(d) t=4.2 ms, $\theta_w = 18.1°$,$\phi = 49.7°$ (e) Reflected wave on wedge (f) Steady disgorged system

FIGURE 11. High-speed images for dynamic RR → MR transition at $M = 1.93$

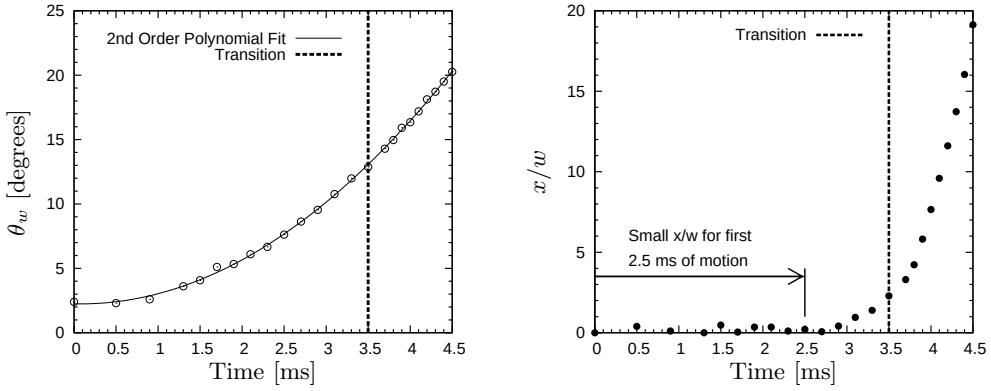

(a) (b)

FIGURE 12. (a) Measured motion of symmetric wedge system and (b) upstream movement of reflection/triple point for dynamic RR → MR transition at $M = 1.93$

5.2. *Strong-reflection range*

As the point of transition in the strong-reflection range is dependent on the level of tunnel free stream turbulence and is tunnel dependent, baseline measurements for the steady experiment were necessary. In figure 15(b) the von Neumann and detachment conditions are indicated ϕ_N and ϕ_D respectively. The dual solution domain is $\phi_N < \phi < \phi_D$. The solid lines in figure 15(b) are second-order polynomial fits through each data set and

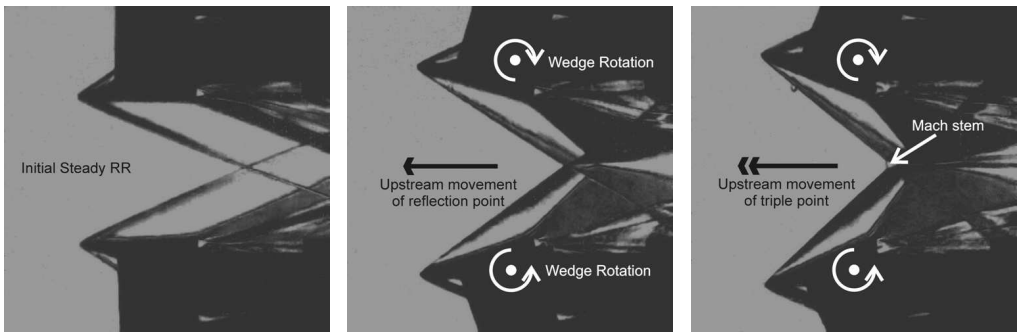

(a) t=0.0 ms,$\theta_w = 2.0°$,$\phi = 23.2°$ (b) t=4.0 ms,$\theta_w = 18.6°$,$\phi = 35.3°$ (c) t=4.7ms,$\theta_w = 24.3°$,$\phi = 41.8°$

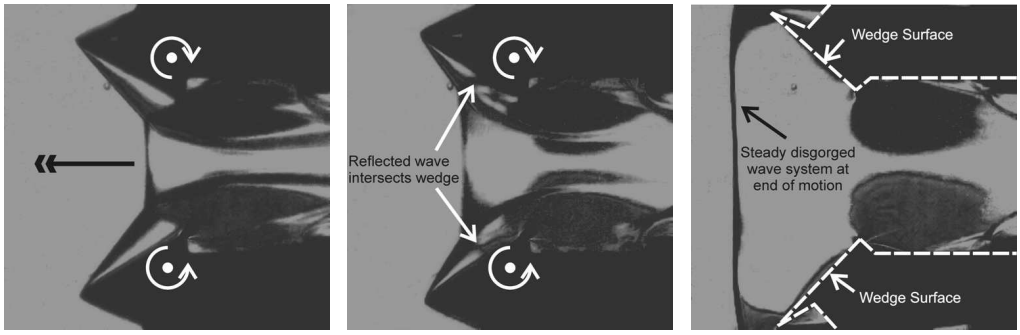

(d) t=5.4ms,$\theta_w = 31.1°$,$\phi = 51.5°$ (e) Reflected wave on wedge (f) Steady disgorged system

FIGURE 13. High-speed images for dynamic RR → MR transition at $M = 2.98$

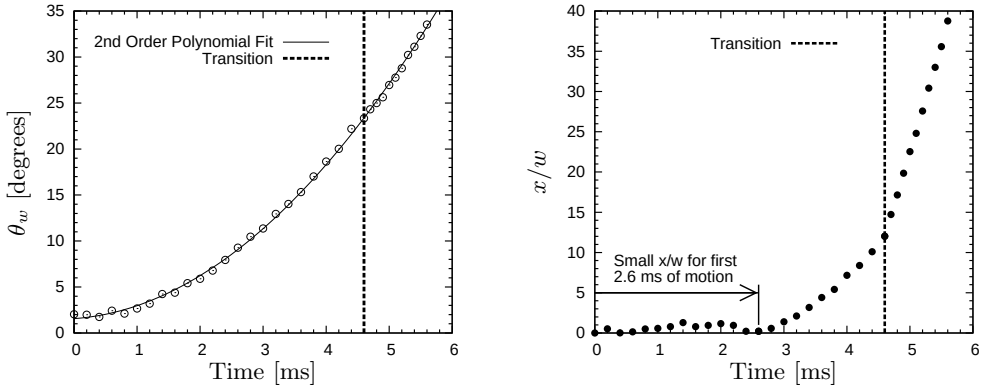

FIGURE 14. (a) Measured motion of symmetric wedge system and (b) upstream movement of reflection/triple point for dynamic RR → MR transition at $M = 2.98$

are used to extrapolate ϕ_T at zero m/w. In the steady experiment, RR ↔ MR takes place close to the von Neumann condition in both directions, indicating that the noise in the CSIR supersonic tunnel is sufficient to suppress hysteresis. For the dynamic case the wedge achieved an instantaneous rotation speed (≈ 9000.0 deg/s) that resulted in $M_E = 0.028$ at the point of transition. The average M_E up to the point of transition was approximately 0.015. The measured ϕ_T for the dynamic experiment is labelled "X".

Analytical steady detachment condition, ϕ_D	43.2°
Measured relative Mach number of reflection point at transition	+ 0.017
Corrected analytical steady detachment condition, ϕ_{DC}	43.1°
Experiment : steady state ϕ_T	43.4°
Experiment : dynamic ϕ_T	44.4°
2D Euler CFD : steady state ϕ_T	43.4°
2D Euler CFD : dynamic ϕ_T	44.3°
Difference between dynamic ϕ_T and ϕ_{DC} (Experiment and CFD)	$\approx 1.2^\circ - 1.3^\circ$

TABLE 3. Summary of ϕ_T from steady and dynamic experiment and CFD at $M = 1.93$, $g/w \approx 0.6$

Analytical steady von Neumann condition, ϕ_N	37.5°
Analytical steady detachment condition, ϕ_D	39.5°
Measured relative Mach number of reflection point at transition	+ 0.046
Corrected analytical steady detachment condition, ϕ_{DC}	39.5°
Experiment : steady state ϕ_T	37.4°
Experiment : dynamic ϕ_T	40.75°
2D Euler CFD : steady state ϕ_T	37.5°
2D Euler CFD : dynamic ϕ_T	40.45°
Difference between dynamic ϕ_T and ϕ_{DC} (CFD and Experiment)	$\approx 0.9^\circ - 1.2^\circ$

TABLE 4. Summary of ϕ_T from steady and dynamic experiment and CFD at $M = 2.98$, $g/w \approx 0.6$

Figure 15(b) shows, very clearly, that the rapid wedge rotation was sufficient to maintain RR past $\phi_T \approx \phi_N$ observed in the steady experiment, through the dual solution domain (as hypothesised by Hornung (1997)) and even beyond ϕ_D. Both the experiment and CFD show that RR persisted approximately $0.9^\circ - 1.2^\circ$ beyond ϕ_{DC}. Once again, there is close agreement between the experimental and computed values of ϕ_T for the dynamic case. The characteristic difference between the two and three-dimensional result is also seen here. This result provides experimental evidence to support the dynamic effect originally computed by Felthun & Skews (2004). Rapid wedge rotation introduces a dynamic effect that delays RR $\rightarrow$ MR transition beyond the steady, theoretical transition condition.

6. Computational simulation of impulsive rotation at $M = 2.98$

The close agreement between experiment and computation provides confidence in the use of flow simulations to investigate the dynamics of the flow field, including the dynamic RR $\rightarrow$ MR transition mechanism. This section analyses two-dimensional Euler CFD results from the simulation of a rapidly rotating wedge in a $M = 2.98$ free stream, started impulsively from a steady, initial RR at $\theta_{wi} = 19.0^\circ$ and rotated continuously at $M_E = 0.1$ (rotation speed = 32644 deg/s with $T_O = 302.3K$ and w= 40.0 mm) until transition to MR. The wedge is rotated about the model rotation centre as illustrated in figure 9. The large rotation speed is implemented deliberately to highlight the resultant transient effects.

6.1. *Dynamic flow solution*

Selected images from the flow solution (flow field density contours) of the impulsive rotation case are presented in figure 16. An initial steady RR is established at an initial

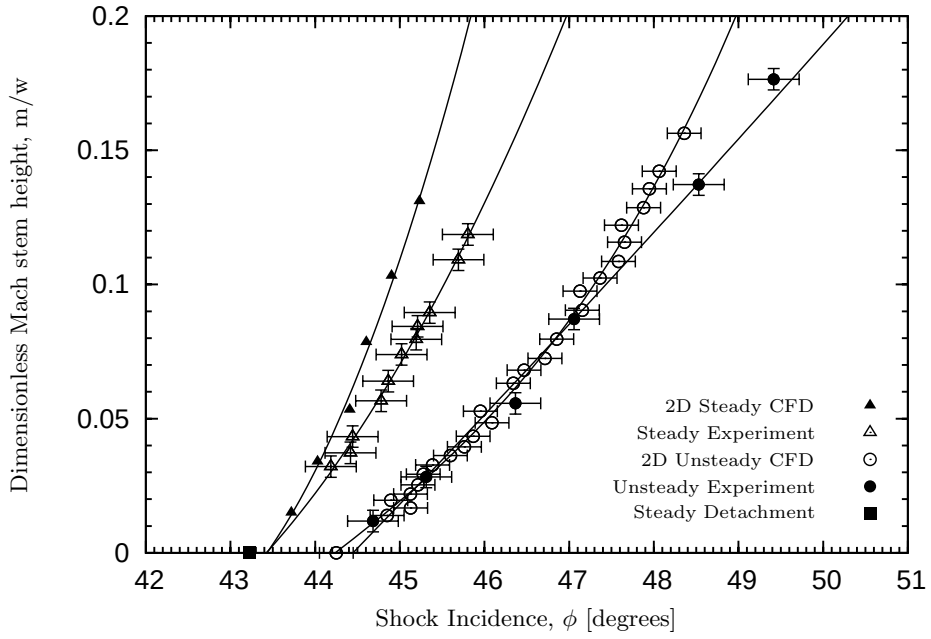

(a) Experimental and CFD results at $M = 1.93$

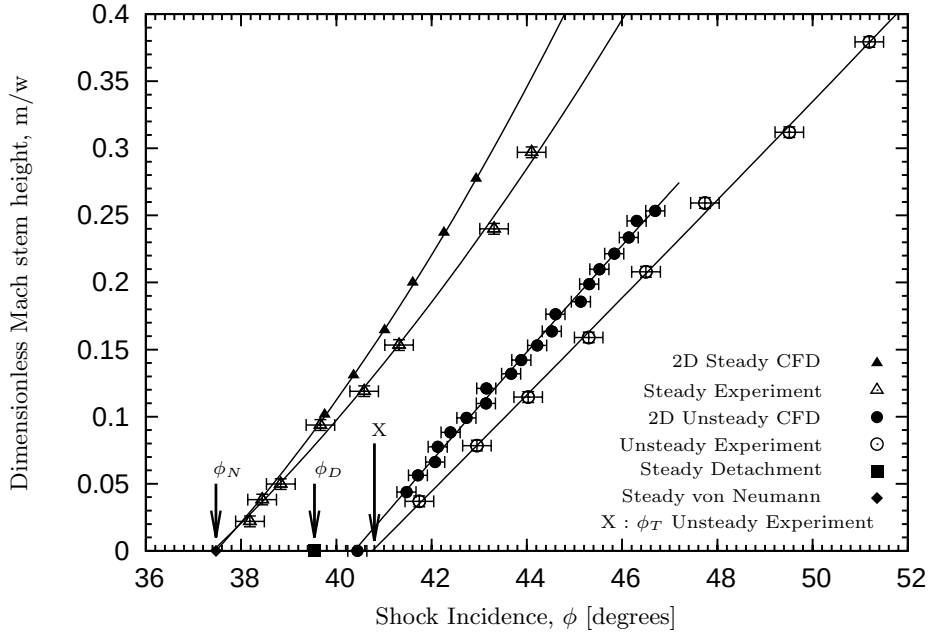

(b) Experimental and CFD results at $M = 2.98$

FIGURE 15. Experimental and CFD results for steady and dynamic RR → MR transition at $M = 1.93$ and 2.98. Solid lines are second-order polynomial fits through each data set and are used to predict ϕ_T at zero m/w.

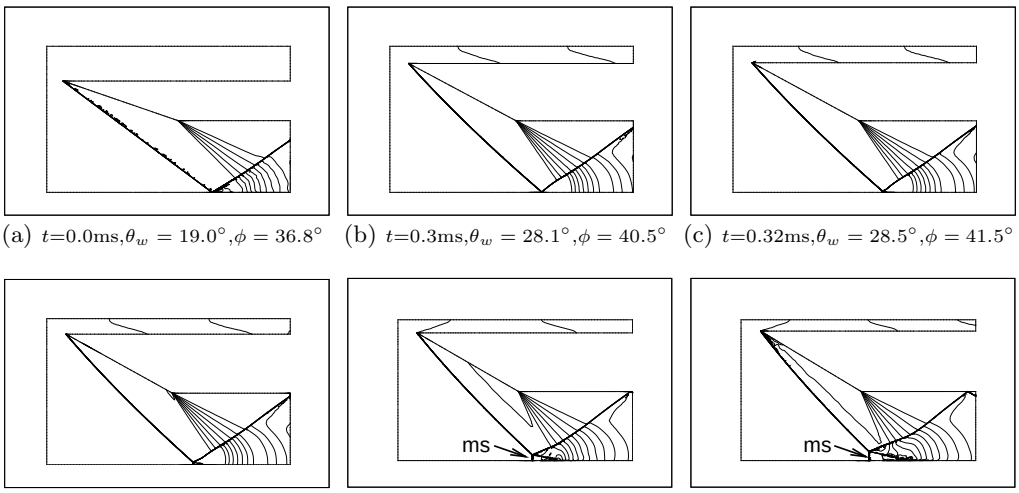

(a) t=0.0ms,$\theta_w = 19.0°$,$\phi = 36.8°$ (b) t=0.3ms,$\theta_w = 28.1°$,$\phi = 40.5°$ (c) t=0.32ms,$\theta_w = 28.5°$,$\phi = 41.5°$

(d) t=0.33ms,$\theta_w = 29.0°$,$\phi = 42.5°$ (e) t=0.37ms,$\theta_w = 30.0°$,$\phi = 43.3°$ (f) t=0.4ms,$\theta_w = 31.0°$,$\phi = 44.9°$

FIGURE 16. Computed density contours showing the flow field development for $M_E = 0.1$, $\theta_{wi} = 19.0°$ at $M = 2.98$, $g/w \approx 0.6$, $T_O \approx 302.3K$. The Mach stem is indicated "ms" only where clearly visible. This is not to be mistaken to indicate the point of transition.

wedge incidence, $\theta_{wi} = 19.0°$, before the wedge is rotated impulsively at a constant rotation speed such that the leading edge speed is 10% of the free stream acoustic speed, i.e. $M_E = 0.1$. As the wedge incidence increases, curvature develops on the incident wave as observed previously by Khotyanovsky et al. (1999) and Felthun & Skews (2004). The visible Mach stems are indicated in figures 16(e) and 16(f). However, the point of transition cannot be identified accurately from the views presented in figure 16. Closeup views of the reflection pattern at $\theta_w = 28.0°$ and $\theta_w = 28.2°$ in figures 17(a) and 17(b) show the early development of the shear layer from the triple point as transition to MR occurs.

Transition is assumed when $\theta_w = 27.9°$, i.e. 0.1° before the appearance of the shear layer in figure 17(a). The corresponding $\phi_T \approx 40.5°$ and $\phi_{DC} = 39.4°$. Transition is delayed with respect to ϕ_{DC} by approximately 1.1°.

Pressure traces through the reflection/triple point are analysed with respect to the steady state pressure-deflection shock polars presented earlier in figure 3. Consider the selection of pressure traces through the reflection/triple point in figure 18. The pressure rise through the reflection point at the steady, initial condition at $\theta_{wi} = 19.0°$ is close to the steady, analytical solution given by point "A" on reflected polar "I" in figure 3, i.e. $P/P_\infty = 9.6$. As the wedge rotates (increasing wedge incidence), the pressure rise through the reflection point increases and peaks at $\theta_w = 27.8°$ with $P/P_\infty \approx 19.0$ in comparison to 13.3 in the steady case (point "C" at the detachment condition on reflected polar "III"). Beyond $\theta_w = 27.8°$ there is a significant drop in pressure. The wedge incidence at which the maximum pressure rise through the reflection point was observed in figure 18 is close to the wedge incidence at which transition was assumed. It is reasonable to assume that the significant drop in pressure is associated with transition to MR, as in the steady case just beyond the detachment condition. Due to this similarity in trend between the dynamic and steady case, pressure-deflection shock polars may be useful in identifying the critical trend that highlights the point of transition.

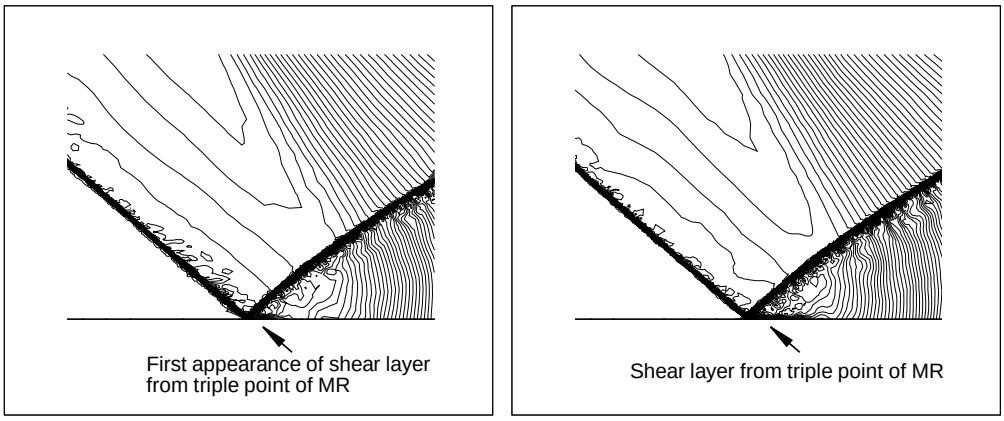

(a) $\theta_w = 28.0^\circ$ (b) $\theta_w = 28.2^\circ$

FIGURE 17. Closeup views of computed density contours showing the first traces of the shear layer from the triple point as the reflection transitions to MR

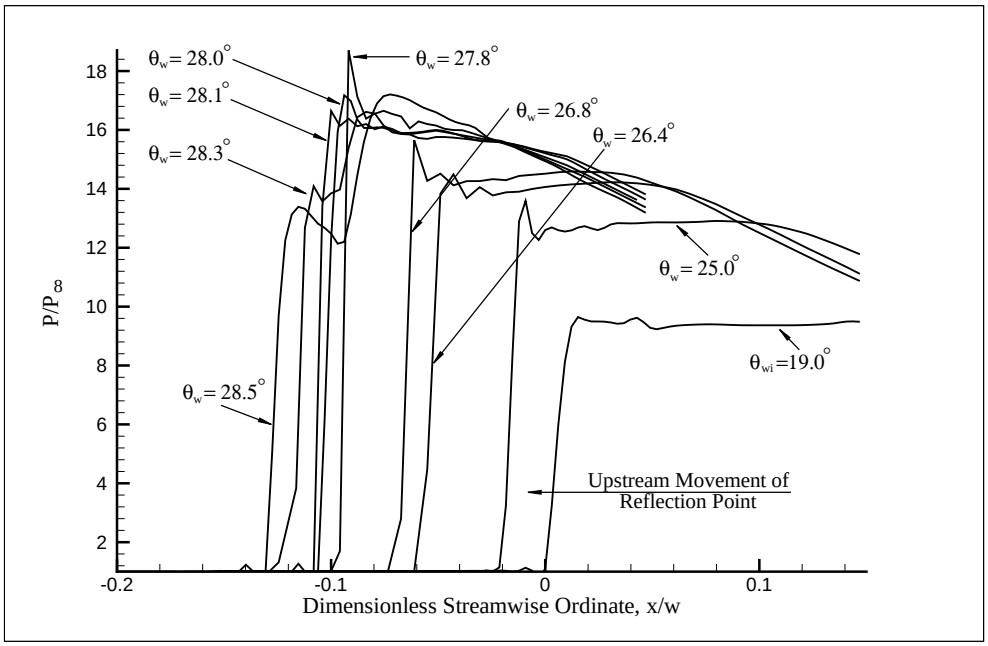

FIGURE 18. Computed pressure traces through the reflection point as the wedge rotates from $\theta_{wi} = 19.0^\circ$ at $M_E = 0.1$ about the model pivot point at $M = 2.98$, $g/w \approx 0.6$

7. Transition criterion and mechanism for dynamic regular to Mach reflection transition

Once again, consider the impulsive rotation case at $M = 2.98$ in the previous section to explore the dynamic RR → MR transition mechanism. Transition was identified at $\theta_w = 27.9^\circ$ in the previous section. From observations of the Mach number contours in the CFD solution, the first time the flow downstream of the reflection point goes sonic is when $\theta_w \approx 26.2^\circ$ as shown in figure 19(a), approximately 1.7° below transition. The subsonic region is highlighted in black as indicated. The leading edge of the expansion intersects the reflected wave downstream of this subsonic region and the length scale

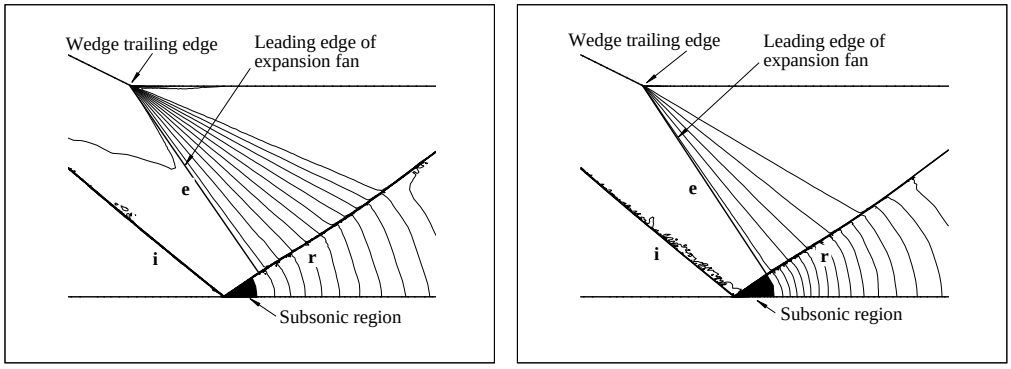

(a) Sonic condition at $\theta_w = \theta_S = 26.2°$

(b) Point of first contact between the expansion fan and the subsonic region at $\theta_w = \theta_C = 26.4°$

FIGURE 19. Computed density contours showing the development of the subsonic region downstream of reflection point before transition at $M = 2.98$, $M_E = 0.1$, $\theta_{wi} = 19.0°$. The subsonic region downstream of the reflection point is shaded black.

cannot be communicated to the reflection point. For convenience this will be referred to as the sonic condition and is labelled θ_S. As the wedge incidence increases, the leading edge of the expansion moves closer to the reflection point and the subsonic region grows until they interact at approximately $\theta_w = 26.4°$ in figure 19(b). This is the smallest incidence at which there is an established communication path between the trailing edge expansion and the reflection point and shall be referred to as θ_C for convenience. Taking into account the local acoustic speed in the subsonic zone, the wedge rotation speed and the finite time it takes the length scale information from the expansion fan to traverse the subsonic region, a prediction can be made as to when the length scale information reaches the reflection point. The wedge rotates to approximately $\theta_w = 26.8°$ as the length scale information reaches the reflection point, approximately 0.6° after the sonic condition. For convenience this will be referred to as the length scale condition and shall be identified by θ_L. Transition was identified earlier at $\theta_w = 27.9°$, approximately 1.1° beyond the identified length scale condition at θ_L. Though the wedge length scale is visible at the reflection point from $\theta_L = 26.8°$, RR persists until transition at $\theta_w = 27.9°$. Therefore, transition to MR must occur when the reflected wave can no longer turn the flow downstream of the incident wave parallel to the reflection plane at the reflection point, i.e. the dynamic equivalent of the detachment condition.

The difference between the sonic and length scale conditions was even more pronounced at $M = 1.93$ as seen in figure 20 in which the wedge was rotated at a constant rotation speed about its trailing edge at $M_E = 0.05$ with $\theta_{wi} = 8.0°$. The first time the flow downstream of the reflection point goes sonic is at approximately $\theta_w = 16.2°$. The subsonic region grows in size until it meets the trailing edge expansion approximately 1.0° later at $\theta_w = 17.2°$. At this point the information still has to traverse the subsonic patch.

In the ideal, steady case the difference between the length scale and detachment conditions is negligible. However, these results show that the difference is more significant for the dynamic case presented. Also, in the ideal steady case, the sonic condition and the length scale condition are synonymous. There is a difference between the two in the dynamic case due to the transient nature of the flow. As illustrated in figure 20, it is possible to increase the time between the sonic condition and the length scale condition.

In summary, for the dynamic case investigated here, the criterion for dynamic RR

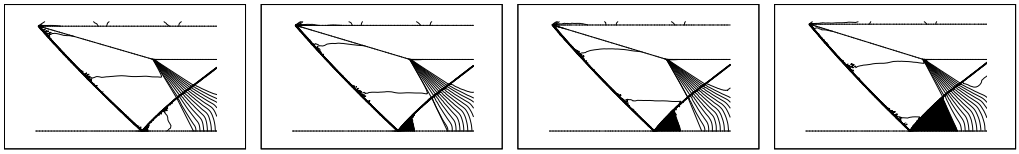

(a) $\theta_w = \theta_S = 16.2°$ (b) $\theta_w = 16.6°$ (c) $\theta_w = 16.8°$ (d) $\theta_w = \theta_C = 17.2°$

FIGURE 20. Computed density contours showing the development of the subsonic region downstream of the reflection point between θ_S and θ_C at $M = 1.93$, $M_E = 0.05$, $\theta_{wi} = 8.0°$. The subsonic region downstream of the reflection point is shaded black.

θ_{wi} [degrees]	*PivotPoint*	ϕ_T [degrees]	g/w	h/w
11.0	Leading Edge	40.9	-	0.91
19.0	Leading Edge	41.3	-	0.91
11.0	Trailing Edge	40.5	0.6	-
19.0	Trailing Edge	40.8	0.6	-

TABLE 5. Computed effect of θ_{wi} on ϕ_T for RR → MR transition at $M_E = 0.1$, $M = 2.98$

→ MR transition is neither the sonic or length scale condition, but rather the dynamic equivalent of the detachment condition.

8. Parameter investigation : dynamic regular to Mach reflection transition

Euler simulations were used to investigate the effect of various parameters, viz. rotation speed, pivot point and initial incidence. Unless otherwise stated, $\theta_{wi} = 19.0°$, $g/w = 0.6$ for pivot about the trailing edge and $h/w = 0.91$ for rotation about the leading edge, where h is the separation of the wedge leading edge from the symmetry plane (see figure 2 for geometric definitions). Results are presented in figure 21 and table 5. The corrected detachment conditions that account for the speed of the reflection point at transition are also plotted. The difference in θ_{DC} and ϕ_{DC} between rotation about the leading and trailing edges is due to the difference in speed of the reflection point at the point of transition. For the range of rotation speeds investigated, the wedge incidence at transition, θ_{WT}, increased for an increase in M_E. The difference in computed ϕ_T between the pivot point in the experiment and the trailing edge is very small and in the order of $0.1°$. The largest difference in ϕ_T is between rotation about the trailing or leading edge, at $M_E = 0.1$. Rapid rotation about the leading edge for $M_E = 0.1$ can delay transition approximately $1.9°$ beyond ϕ_{DC} whereas rapid rotation about the trailing edge can delay transition by approximately $1.4°$ beyond ϕ_{DC}. Two initial conditions were tested for rotation about the trailing and leading edges to determine if there was any dependence on initial incidence. Table 5 summarises the results and shows that the difference in ϕ_T ($40.9° - 41.3°$ and $40.5° - 40.8°$) is just outside the uncertainty $\delta\phi = \pm 0.2°$ documented in section 4.1. The dynamics of the rapidly rotating wedge are complex and it would be incorrect to draw a general conclusion about the influence of initial incidence on the point of transition from these four tests. The same could be said for rotation speed. The primary purpose of this limited series of tests was to identify dependent variables in the parameter space and to determine the order of magnitude of their influence in a limited range.

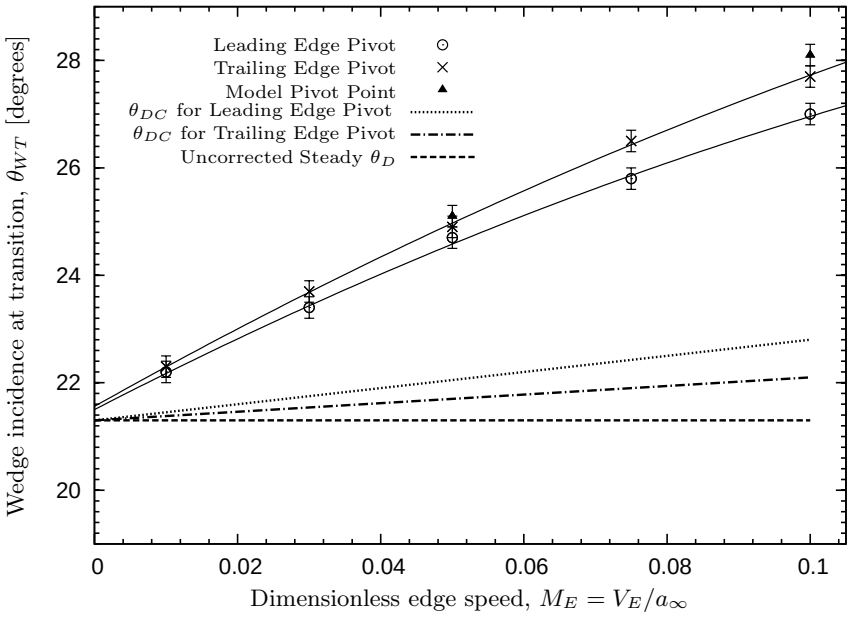

(a) Transition wedge incidence vs. dimensionless edge speed

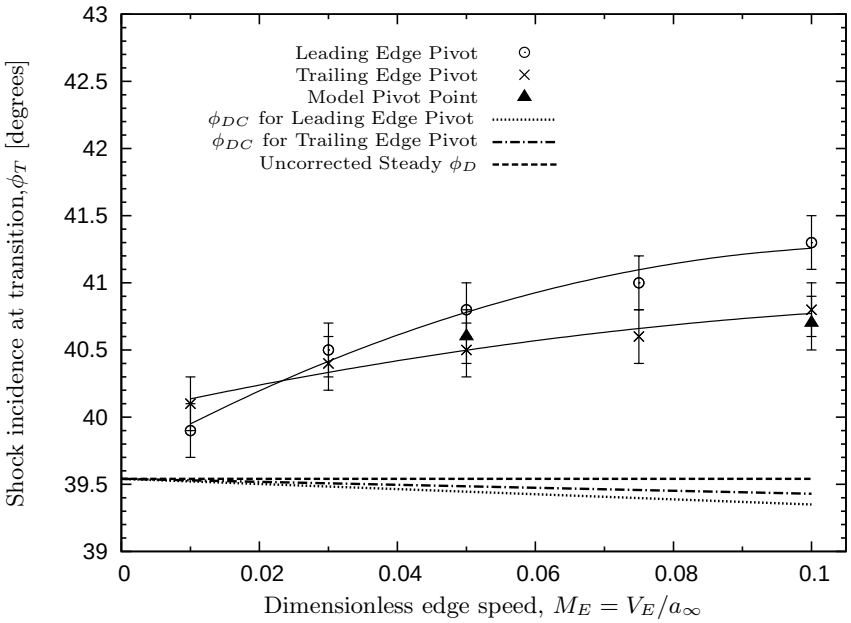

(b) Transition shock incidence vs. dimensionless edge speed

FIGURE 21. Computed variation of θ_{WT} and ϕ_T with M_E for RR $\rightarrow$ MR transition at $M = 2.98$, $\theta_{wi} = 19.0^\circ$. The solid lines are second-order polynomial fits to the computed values of θ_{WT} and ϕ_T for rotation about the leading and trailing edges.

M	P_O [kPa]	T_O [K]	ϕ_i [degrees]
2.96	474.0	301.0	41.2
3.26	616.0	302.0	40.2

TABLE 6. Experiment test conditions for dynamic MR → RR transition experiments, $g/w \approx 0.6$

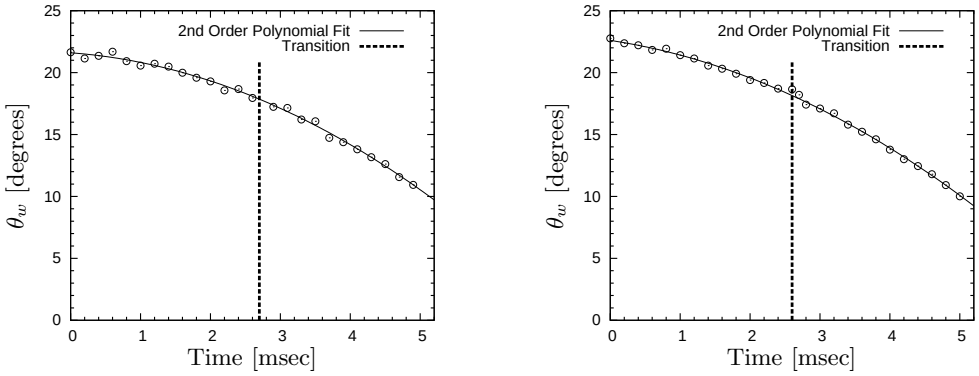

(a) $M = 2.96$ (b) $M = 3.26$

FIGURE 22. Measured motion of symmetric wedge system for MR → RR transition

Analytical steady von Neumann condition, ϕ_N	36.2°
Measured relative Mach number of reflection point at transition	- 0.03
Corrected analytical steady von Neumann condition, ϕ_{NC}	36.3°
Experiment : dynamic ϕ_T	35.5°
2D Euler CFD : steady state ϕ_T	36.2°
2D Euler CFD : dynamic ϕ_T	35.5°
Difference between dynamic ϕ_T and ϕ_{NC} (CFD and Experiment)	$\approx 0.8°$

TABLE 7. Experimental and CFD results for steady and dynamic MR → RR transition at $M = 3.26$, $g/w \approx 0.6$.

9. Experimental results for dynamic Mach to regular reflection transition

Experiments for dynamic MR → RR transition were done at $M = 3.26$ and 2.96. The spring-driven actuator was installed to decrease wedge incidence rapidly on latch release. Experiment test conditions are included in table 6. The measured wedge motion is documented in figure 22. In both experiments RR persisted below ϕ_{NC}. There is no fundamental difference between the two cases in terms of flow physics. Only results for the $M = 3.26$ case are analysed in some detail. Select high-speed images for the experiment at $M = 3.26$ are presented in figure 23. Figure 25 includes ϕ_T from both experiments against the steady theoretical transition criteria. Zero time corresponds to the image frame just before any wedge movement is visible on the high-speed images.

After tunnel startup, an initial, steady MR was set up just beyond the dual solution domain (figure 23(a)) after which time the wedge incidence was reduced rapidly. As θ_w decreases, the Mach stem moves downstream and the Mach stem height decreases

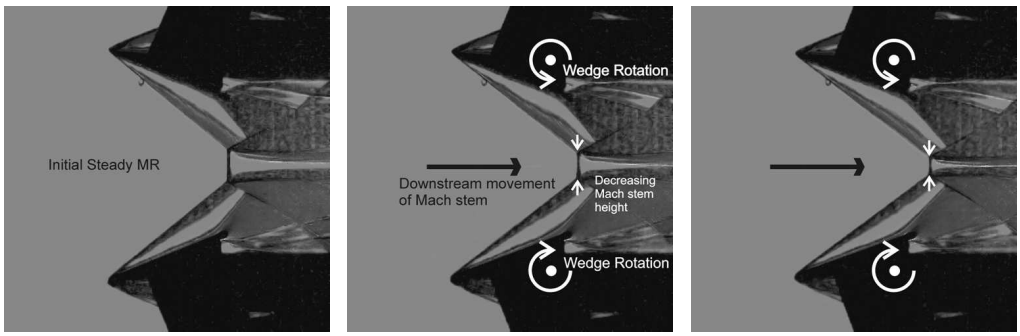

(a) t =0.0 ms,$\theta_w = 22.8°$,$\phi = 40.2°$ (b) t=1.1 ms,$\theta_w = 21.4°$,$\phi = 39.0°$ (c) t=1.7 ms,$\theta_w = 20.3°$,$\phi = 37.8°$

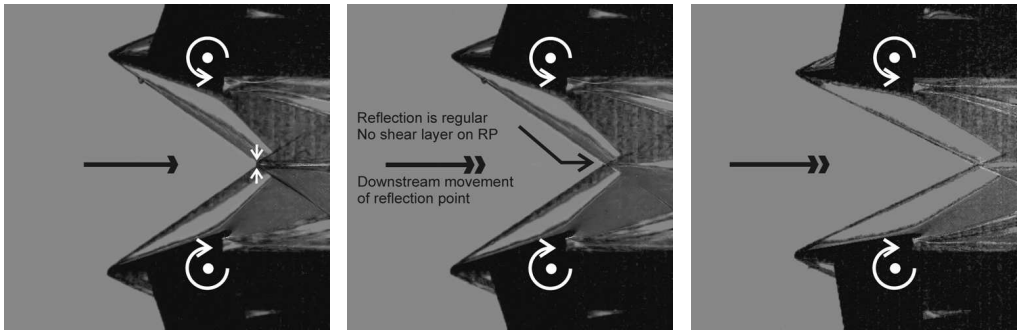

(d) t=2.5 ms,$\theta_w = 18.7°$,$\phi = 35.9°$ (e) t=2.8 ms,$\theta_w = 18.2°$,$\phi = 35.1°$ (f) t=5.2 ms,$\theta_w = 9.2°$,$\phi = 26.2°$

FIGURE 23. High-speed images for dynamic MR → RR transition at $M = 3.26$

(figures 23(b) - 23(d)) until transition to RR. In figure 23(e) the reflection pattern is clearly RR. The wedge rotation continues well after transition, but the flow field after transition is not analysed further here. The instantaneous rotation speed at the point of transition was approximately 2500 deg/s with $M_E = 0.008$, approximately 0.8% of the free stream acoustic speed. The tunnel conditions, measured wedge motion and ϕ_i were used as inputs to the CFD simulation. The experimental and computed Mach stem height variation with shock incidence angle is presented in figure 24. A linear fit to both data sets, only for $\phi \leqslant 38.0°$, is used to extrapolate ϕ_T at zero m/w. As indicated on the graph, the expected, initial difference in Mach stem height between the CFD and experiment is evident, though small at this initial condition (labelled m/w_{iCFD} and m/w_{iexp} respectively). As the wedge rotates there is a deviation from the steady case as indicated by "A" on figure 24. As the Mach stem height decreases, the unsteady CFD and experiment converge to $\phi_T \approx 35.5°$. The analytical transition condition was corrected for the speed of the triple point at transition and results are summarised in table 7. Transition was observed approximately 0.8° below ϕ_{NC} and there is close agreement on ϕ_T between the experiment and computation. Though the rotation speeds achieved here were not as large as in the RR → MR transition experiments, the dynamic effect of rapid wedge rotation on ϕ_T is still evident.

The Mach stem development from a simulation at the same free stream conditions and ϕ_i, with a larger, but constant rotation about the wedge trailing edge at $M_E = 0.05$ is also plotted in figure 24. The deviation from the steady case is significant. In this instance transition to RR was predicted at $\phi_T \approx 32.7°$, 3.5° below ϕ_N and 4.5° below ϕ_{NC}.

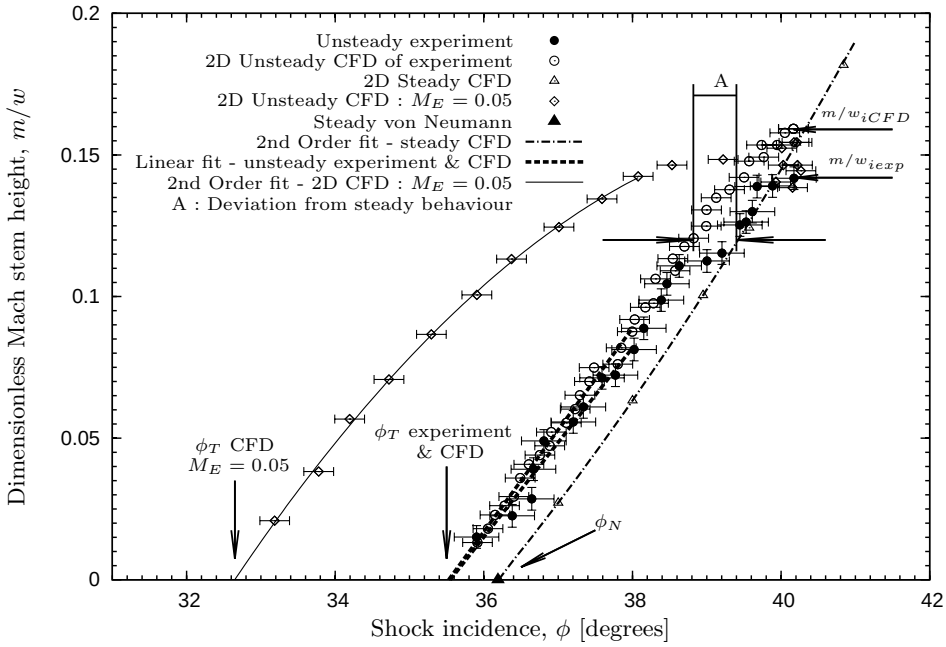

FIGURE 24. Mach stem development from experiment and CFD for dynamic MR → RR transition at $M = 3.26$, $g/w \approx 0.6$. The dashed and solid lines represent first and second-order fits respectively, only for $\phi \leqslant 38.0^\circ$, to their respective data sets and are used to extrapolate ϕ_T at zero m/w. The offset from the steady data due to rapid rotation of the wedge is labelled "A".

10. Conclusions

A rig was designed to investigate the dynamic shock wave reflection phenomena generated by a rapidly rotating wedge. Steady state experiments in the strong-reflection range show that the free stream noise in the CSIR wind tunnel facility is sufficient to suppress hysteresis and transition was observed close to the von Neumann condition for increasing and decreasing wedge incidence. For increasing incidence, it was possible to maintain RR beyond the dual solution domain with rapid rotation. In the dynamic experiments and computations at $M = 1.93$ and 2.98, RR persisted approximately $0.9^\circ - 1.3^\circ$ beyond ϕ_{DC}.

The dynamic RR → MR transition mechanism was investigated with Euler CFD applied to the simulation of an impulsively rotated wedge at $M = 2.98$. For the dynamic case investigated here, a distinction is drawn between the sonic, length scale and "detachment" conditions for dynamic RR → MR transition. Results show that the wedge length scale from the trailing edge expansion is not necessarily communicated to the reflection point as the flow downstream of the reflection point first goes sonic. Computations also show that it is possible for RR to persist beyond the length scale condition. It is possible that RR is maintained beyond the length scale condition as long as the reflected wave is able to maintain the boundary condition at the reflection plane until the dynamic equivalent of the detachment condition. Pressure traces through the reflection point show that rapid rotation increases the maximum achievable pressure rise through the reflection point of a RR in comparison to the steady case.

The parameter investigation showed a dependency on rotation speed. The maximum difference in ϕ_T due to a change in pivot point is in the order of 0.5° at the maximum

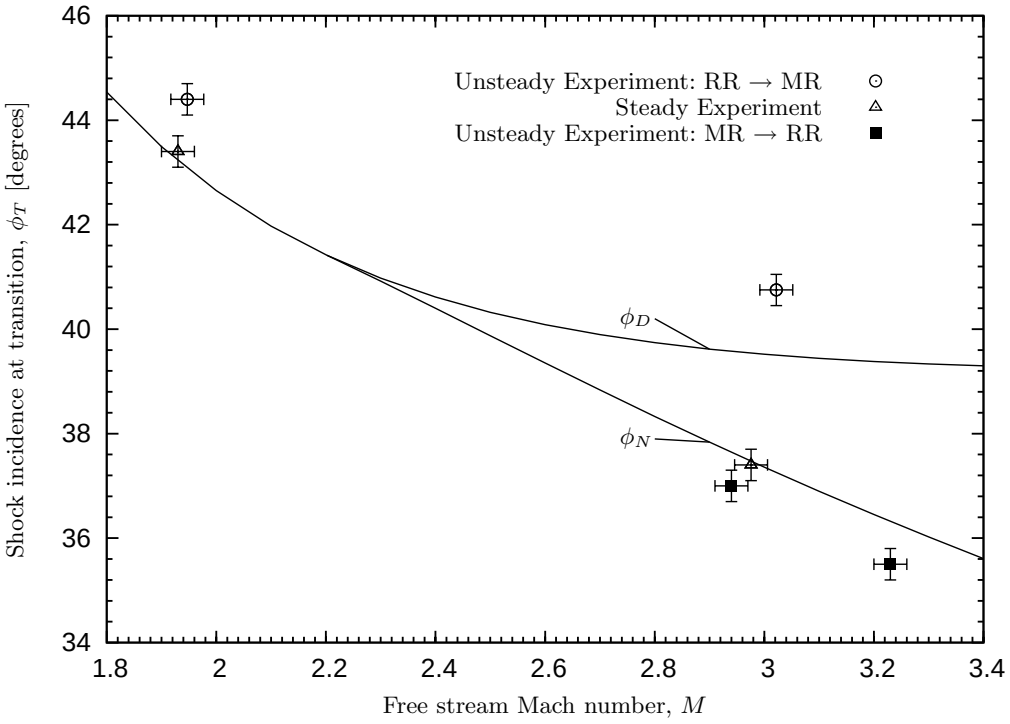

FIGURE 25. Measured ϕ_T from experiments compared to analytical steady transition criteria

rotation speed with $M_E = 0.01$. The difference in ϕ_T due to a change in initial incidence was small and just outside the uncertainty of $\delta\phi = \pm 0.2°$.

In experiments and computations for dynamic MR → RR transition at $M = 3.26$, transition was delayed approximately 0.8° below ϕ_{NC}. Transition to RR may be delayed further by increasing the rotation speed. At $M_E = 0.05$, MR → RR transition was observed approximately 3.5° below ϕ_N and 4.5° below ϕ_{NC}.

We would like to acknowledge the support of South Africa's Council for Scientific and Industrial Research, the Defence, Peace, Safety and Security Unit and South Africa's Department of Science and Technology.

REFERENCES

AZEVEDO, D. J. & LIU, C. S. 1993 Engineering approach to the prediction of shock patterns in bounded high-speed flows. *AIAA J.* **31**, 83–90.

BEN-DOR, G. 2007 *Shock Wave Reflection Phenomena*. Springer.

BEN-DOR, G. 1999 Hysteresis phenomena in shock wave reflections in steady flows. In *Proc. 22nd Intl Symp. on Shock Waves* (ed. G. J. Ball, R. Hillier, G. T. Roberts). Paper 6000.

BEN-DOR, G., IVANOV, M., VASILEV, E.I., ELPERIN, T. 2002 Hysteresis processes in the regular reflection ↔ Mach reflection transition in steady flows. *Progress in Aerospace Sciences* **38**, 347–387.

CHPOUN, A., BEN-DOR, G. 1995 Numerical confirmation of the hysteresis phenomenon in the regular to Mach reflection transition in steady flows. *Shock Waves* **5**, 199–203.

FELTHUN, L. T. & SKEWS, B. W. 2004 Dynamic shock wave reflection. *AIAA J.* **42**, 1633–1639.

Henderson, L. F., Lozzi, A. 1979 Further experiments on transition to Mach reflexion. *J. Fluid Mech.* **94**, 541–559.

Hornung, H. G., Oertel, H., Sandeman, R. J 1979 Transition to Mach reflection of shock-waves in steady and pseudo-steady flow with and without relaxation. *J. Fluid Mech.* **90**, 541–560.

Hornung, H. G. & Robinson, M. L. 1982 Transition from regular to Mach reflection of shock waves. Part 2. The steady flow criterion. *J. Fluid Mech.* **123**, 155–164.

Hornung, H. G. 1986 Regular and Mach reflection of shock waves. *Annual Review of Fluid Mechanics* **18**, 33–58.

Hornung, H. G. 1997 On the stability of steady-flow regular and Mach reflection *Shock Waves* **7**, 123–125.

Ivanov, M. S., Gimelshein, S. F., Beylich, A. E. 1995 Hysteresis effect in stationary reflection of shock-waves. *Phys. Fluids* **7**, 685–687.

Ivanov, M. S., Zeitoun, D., Vuillon, J., Gimelshein, S. F., Markelov, G. N. 1996 Investigation of the Hysteresis Phenomena in Steady Shock Reflection Using Kinetic and Continuum Methods. *Shock Waves* **5**, 341–346.

Ivanov, M. S., Markelov, G. N., Kudryavtsev, A. N., Gimelshein, S. F. 1998 Numerical Analysis of Shock Wave Reflection Transition in Steady Flows. *AIAA J.* **36**, 2079–2086.

Ivanov, M. S., Vandromme, D., Fomin, V. M., Kudryavtsev, A. N., Hadjadj, A., Khotyanovsky, D. V. 2001 Transition between regular and Mach reflection of shock waves: new numerical and experimental results. *Shock Waves* **11**, 199–207.

Ivanov, M. S., Kudryavtsev, A. N., Nikiforov, S. B., Khotyanovsky, D. V., Pavlov, A. A. 2003 Experiments on shock wave reflection transition and hysteresis in a low-noise wind tunnel. *Phys. Fluids* **15**, 1807–1810.

Khotyanovsky, D. V., Kudryavtsev, A. N., Ivanov, M. S. 1999 Numerical study of transition between steady regular and Mach reflection caused by free-stream perturbations. In *Proc. 22nd Intl Symp. on Shock Waves* (ed. G. J. Ball, R. Hillier, G. T. Roberts).

Kudryavtsev, A. N., Khotyanovsky, D. V., Ivanov, M. S., Hadjadj, A., Vandromme, D. 2002 Numerical investigations of transition between regular and Mach reflections caused by free-stream disturbances. *Shock Waves* **12**, 157–165.

Li, H., Chpoun, A., Ben-Dor, G. 1999 Analytical and experimental investigations of the reflection of asymmetric shock waves in steady flows. *J. Fluid Mech.* **390**, 25–43.

Liou, M. 1996 A sequel to AUSM: AUSM+. *J. Comp. Phys.* **129**, 364–382.

Markelov, G. N., Pivkin, I. V., Ivanov, M. S. 1999 Impulsive Wedge Rotation Effects on Transition from Regular to Mach Reflection. In *Proc. 22nd Intl Symp. on Shock Waves* (ed. G. J. Ball, R. Hillier, G. T. Roberts).

Mouton, C. A., Hornung, H. G. 2007 Mach stem height and growth rate predictions. *AIAA J.* **45**, 1977–1987.

Mouton, C. A., Hornung, H. G. 2008 Experiments on the mechanism of inducing transition between regular and Mach reflection. *Phys. Fluids* **20**, 126103:1–11.

Settles, G. S. 2001 *Schlieren and Shadowgraph Techniques:Visualising Phenomena in Transparent Media*. Springer.

Skews, B. W 1997 Aspect ratio effects in wind tunnel studies of shock wave reflection transition. *Shock Waves* **7**, 373–383.

Skews, B. W. 2000 Three dimensional effects in wind tunnel studies of shock wave reflection. *J. Fluid Mech.* **407**, 85–104.

Sudani, N., Sato, M., Karasawa, T., Noda, J., Tate, A., Watanabe, M. 2002 Irregular effects on the transition from regular to Mach reflection of shock waves in wind tunnel flows. *J. Fluid Mech.* **459**, 167–185.

Vuillon, J., Zeitoun, D., Ben-Dor, G. 1995 Reconsideration of oblique shock wave reflection in steady flows. Part 2. Numerical investigation. *J. Fluid Mech.* **301**, 37–50.